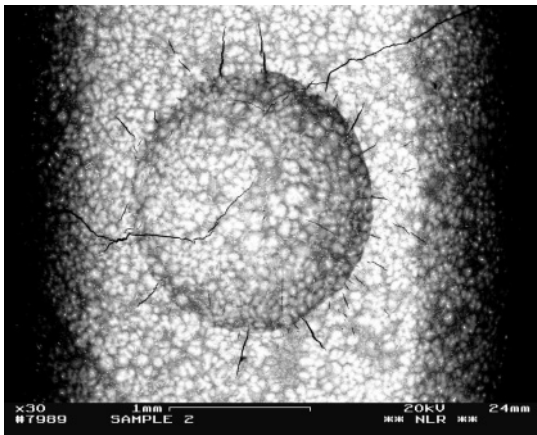




Executive summary

Foreign Object Damage effects on High-Cycle Fatigue of a γ -TiAl alloy



Foreign Object Damage (indent and cracks) on the surface of a γ -TiAl alloy

Problem area

Effect of Foreign Object Damage (FOD) on High-Cycle Fatigue (HCF) of γ -TiAl turbine blades.

Description of the work

Effects of FOD on HCF of a commercial γ -TiAl alloy were investigated and the results analysed using Kitagawa-Takahashi (K-T) diagrams.

Results and conclusions

γ -TiAl HCF strengths are highly sensitive to FOD. K-T diagrams have difficulty in providing boundaries between HCF *crack growth* and *no crack growth*.

Report no.

NLR-TP-2006-154

Author(s)

R.J.H. Wanhill
J.-P.H.M. Steijaert
M.F.J. Koolloos

Classification report

Unclassified

Date

March 2006

Knowledge area(s)

Vliegtuigmateriaal- en schadeonderzoek

Descriptor(s)

Foreign Object Damage
fatigue
gamma titanium aluminide



NLR-TP-2006-154




Foreign Object Damage effects on High-Cycle Fatigue of a γ -TiAl alloy

R.J.H Wanhill, J.-P.H.M. Steijaert and M.F.J. Koolloos

This report may be cited on condition that full credit is given to NLR and the authors.

| | |
|-------------------------|-----------------------------------|
| Customer | National Aerospace Laboratory NLR |
| Contract number | WP S.1.B.3 |
| Owner | National Aerospace Laboratory NLR |
| Division | Aerospace Vehicles |
| Distribution | Unlimited |
| Classification of title | Unclassified |

Approved by:

| | | |
|--|--|---|
| Author  21/04/06 | Reviewer  24/4 | Managing department  BO |
|--|--|---|



Summary

The effects of Foreign Object Damage (FOD) on High-Cycle Fatigue (HCF) of a commercial γ -TiAl alloy were investigated. Specimens prepared from a low-pressure turbine blade were impacted by steel balls at different velocities. After heat-tinting to distinguish FOD-induced cracks, the specimens were tested in HCF to failure. The FOD crack sizes and HCF failure stresses were used to determine the suitability of Kitagawa-Takahashi (K-T) diagrams for providing boundaries between the conditions of *crack growth* and *no crack growth* in HCF.

Contents

| | |
|---|-----------|
| Nomenclature and acronyms | 5 |
| 1. Introduction | 6 |
| 2. Experimental details | 7 |
| 2.1 <i>Material</i> | 7 |
| 2.2 <i>Specimens</i> | 7 |
| 2.3 <i>FOD impact tests</i> | 7 |
| 2.4 <i>Heat-tinting</i> | 7 |
| 2.5 <i>HCF testing</i> | 8 |
| 3. Results | 8 |
| 3.1 <i>FOD impact tests</i> | 8 |
| 3.2 <i>HCF and FOD + HCF tests</i> | 8 |
| 3.3 <i>FOD crack sizes and equivalent crack sizes</i> | 8 |
| 3.4 <i>Impact velocities and HCF failure stresses versus equivalent FOD-induced crack sizes</i> | 9 |
| 4. Analysis with Kitagawa-Takahashi (K-T) diagrams | 9 |
| 5. Concluding remarks and recommendations | 10 |
| 6. Acknowledgements | 10 |
| 7. References | 11 |

3 Tables

10 Figures

(20 pages in total)

Nomenclature and acronyms

| | |
|--------------------|--|
| a | actual crack size |
| a_o | effective crack size (to be added to the actual crack size) |
| FOD | Foreign Object Damage |
| γ -TiAl | gamma titanium aluminide (an intermetallic alloy) |
| HCF | High-Cycle Fatigue |
| HRC | Hardness on the Rockwell “C” scale |
| K-T | Kitagawa-Takahashi (diagram) |
| ΔK_{th} | fatigue crack growth threshold |
| N_b | cycle block size |
| N_f | number of cycles to failure in the final block of cycles |
| R | stress ratio, S_{min}/S_{max} |
| SEM | Scanning Electron Microscope |
| S – N | Stress (fatigue) <i>versus</i> Number of cycles |
| S_{max}, S_{min} | maximum and minimum fatigue stresses |
| ΔS | fatigue failure stress range |
| ΔS_e | HCF endurance limit for smooth, uncracked specimens |
| ΔS_f | cyclic stress range of the final block of cycles |
| ΔS_{f-1} | cyclic stress range of the previous no-failure block of cycles |
| Y | crack geometry factor |

Foreign object damage effects on high-cycle fatigue of a γ -TiAl alloy

R.J.H. Wanhill*, J.-P.H.M. Steijaert, M.F.J. Koolloos

National Aerospace Laboratory NLR, Amsterdam, The Netherlands

Abstract

The effects of Foreign Object Damage (FOD) on High-Cycle Fatigue (HCF) of a commercial γ -TiAl alloy were investigated. Specimens prepared from a low-pressure turbine blade were impacted by steel balls at different velocities. After heat-tinting to distinguish FOD-induced cracks, the specimens were tested in HCF to failure. The FOD crack sizes and HCF failure stresses were used to determine the suitability of Kitagawa-Takahashi (K-T) diagrams for providing boundaries between the conditions of *crack growth* and *no crack growth* in HCF.

Keywords: Foreign Object Damage; fatigue; gamma titanium aluminide

1. Introduction

Since the early 1990's the gamma titanium aluminides (γ -TiAl alloys) have been regarded as candidate materials for gas turbine rotating components operating in the range 550°–700°C. These materials can be modified by alloying additions and processing to achieve good combinations of high-temperature static, fatigue and creep strengths [1–6], and hardware demonstrations have been made [7–9]. On the other hand, γ -TiAl alloys, like all intermetallics, have low ductility and toughness at ambient temperatures, making hardware designers reluctant to consider and use them.

Less obvious is the significance of fatigue when the potential occurrence of fatigue crack growth has to be considered. Although γ -TiAl alloys have relatively high fatigue crack growth rates compared with conventional alloys [10], the most important fatigue consideration for gas turbine rotating components is whether High-Cycle Fatigue (HCF) cracks can initiate [11]. This is because the characteristic high frequency vibratory loads make fatigue crack growth periods too short to enable safety by inspection.

Traditional design against HCF uses fatigue stress *versus* cycles (S – N) data to derive Haigh diagrams, which are modified by imposing experience-based safety factors on the allowable stress levels. This approach is unsuitable for γ -TiAl alloys because their low toughness at ambient temperatures makes them sensitive to cracking from incidental damage. This includes damage caused by small-object impacts [12–14], customarily referred to as Foreign Object Damage (FOD).

An alternative HCF design approach is to determine the limiting fatigue stress levels below which fatigue cracks will not initiate from FOD. This might be possible using Kitagawa-Takahashi (K-T) diagrams [15]. These considerations prompted the present investigation.

* Corresponding author. Tel.: +31-52724-8294; fax: +31-52724-8210
E-mail address: wanhill@nlr.nl

2. Experimental details

2.1 Material

The material was a commercially-developed γ -TiAl alloy designated ABB-23. It was supplied by ALSTOM Power (Switzerland) as the fir-tree root of a fourth stage low-pressure turbine blade from an industrial gas turbine. The blade had been cast, hot isostatically pressed for 4 hr at 1260°C and 172 MPa, and heat-treated in two steps: 1 hr 1350°C, fan cool; 6 hr 1000°C, furnace cool. This resulted in a nearly lamellar microstructure with colony size $350 \pm 100 \mu\text{m}$, see figure 1.

The composition of the alloy, in at. %, was Ti-46.9Al-2.0W-0.53Si-0.06B. The low boron (grain refiner) content is noteworthy. ABB-23 should have a nominal boron content of 0.6 at.%. However, for the present investigation it was useful to have a fairly coarse colony size: see section 4, the analysis description of figure 10b.

2.2 Specimens

The specimen design for FOD + HCF testing had to meet three main requirements: (1) gauge length thickness representing the leading edge of an industrial gas turbine blade; (2) a flat section in the gauge length to provide a constant impact angle; (3) smooth and well-blended edges to prevent stress concentrations other than those due to FOD. Figure 2 shows the final design.

The fir-tree root was electric discharge machined into 12 sections. 17 cylindrical blanks were electric discharge machined from these sections and machined to the specimen geometry. The specimens were carefully mechanically polished to remove any irregularities and reduce/eliminate residual stresses due to machining.

2.3 FOD impact tests

In real FOD events the shape, size, mass, velocity and impact angle of the objects vary. But for experimental purposes the impact events must be reproducible. The limited number of specimens permitted only one variable, the impact velocity.

The specimens were mounted in a support fixture before impact testing, see figure 3. this fixture was needed to simulate the underlying support of a turbine blade leading edge by the mass of the rest of the airfoil. The impact tests were done with a compressed air gun firing a 3 mm diameter hard steel ball, Rockwell HRC 63–66, and with a mass of 0.11g. Similar impacting objects have been used for FOD tests on a conventional titanium alloy [16–18].

Dummy specimen impact tests showed that the impact velocity should be no higher than 250 m/s, otherwise major cracking and even immediate fracture of the specimens would occur. The definitive tests were done with impact velocities of 50, 100, 150, 200 and 250 m/s on duplicate specimens. This left several undamaged specimens for baseline HCF tests.

2.4 Heat-tinting

Heat-tinting was used to determine the sizes and shapes of FOD-induced cracks that led to HCF failure. The heat-tinting conditions were obtained from the results of two sets of dummy tests. First, dummy specimen room temperature HCF tests showed that prior heating for 30 min. at 500°, 600° and 700°C had no effect on the 10^7 cycles fatigue “limit”. Secondly,

dummy specimen FOD + heating + room temperature HCF tests showed that the best contrast between heat-tinted FOD-induced cracks and the HCF fracture surfaces was obtained from heating for 30 min. at 600°C. This heat-tinting condition was used for the definitive FOD + HCF tests.

2.5 HCF testing

For convenience, and because this was a proof-of-concept investigation, the HCF tests were run at room temperature. The tests were done using a Schenck Hydropulse machine, applying constant amplitude sinusoidal loading with stress ratio $R = 0.1$ and a cycle frequency of 15 Hz. Owing to the limited number of FOD + HCF specimens, the fatigue failure stresses were determined from the step test method validated by Bellows *et al.* [19].

The step test method requires testing a specimen with a constant fatigue stress range for a fixed number of cycles, the cycle block. If failure does not occur within this cycle block, the fatigue stress range is increased by a small percentage. This procedure is repeated until failure occurs. For the present HCF tests the block size was 10^5 cycles and the fatigue stress range increment was 18 MPa. The fatigue failure stress range was calculated from [19]:

$$\Delta S = \Delta S_{f-1} + (\Delta S_f - \Delta S_{f-1}) \cdot (N_f / N_b) \quad (1)$$

where ΔS is the fatigue failure stress range; ΔS_{f-1} is the cyclic stress range from the previous no-failure block; ΔS_f is the cyclic stress range of the final block; N_f is the number of cycles to failure in the final block; and N_b is the block size. N.B: a block size of 10^5 cycles is sufficient for materials, like γ -TiAl alloys [4,6,10], which have very flat S – N curves and high fatigue crack growth rates. In other words, if a FOD-induced crack does not grow to failure within 10^5 cycles, it can be assumed that failure will not happen under the current cyclic stress range.

3. Results

3.1 FOD impact tests

Using a Scanning Electron Microscope (SEM) the impact damage from the definitive FOD tests was quantified as shown in figure 4. The results are given in table 1 and demonstrate good reproducibility for impact velocities of 50 – 200 m/s. The 50 m/s impact damage was confined to the indents. On the other hand, one of the 250 m/s impacted specimens broke immediately, despite the dummy test results. Figure 5 presents the averaged main results from table 1, and includes two examples of the observed damage.

3.2 HCF and FOD + HCF tests

Table 2 gives the HCF and FOD + HCF results. These are plotted straightforwardly in figure 6. This shows a linear relationship between the fatigue failure stress range, ΔS , and the impact velocity for the FOD + HCF specimens. Extrapolation of this relationship underestimates the fatigue failure stress ranges of the specimens without FOD. This is unsurprising, since these specimens did not contain indents or cracks before HCF testing.

3.3 FOD crack sizes and equivalent crack sizes

After HCF testing the FOD-induced heat-tinted cracks could be measured from the fracture surfaces. Figure 7 shows two easily observable examples. The FOD-induced cracks were

converted into equivalent semi-circular cracks perpendicular to the principal stress axis, using the $\sqrt{\text{area}}$ method of Murakami for inclined surface cracks of arbitrary shape [20,21]. The results are given in table 3.

3.4 Impact velocities and HCF failure stresses versus equivalent FOD-induced crack sizes

Figure 8 presents plots of impact velocities and fatigue failure stress ranges, ΔS , versus the equivalent FOD-induced crack sizes. Figure 8a shows large scatter, but figure 8b shows a good correlation between ΔS and the equivalent FOD-induced crack size. In the light of the irregularity of the actual FOD-induced cracks, for example figure 7, the good correlation in figure 8b is encouraging for further analysis with K-T diagrams, which necessarily use equivalent crack sizes.

4. Analysis with Kitagawa-Takahashi (K-T) diagrams

As mentioned in the introduction, designing against HCF using Haigh diagrams is unsuitable for γ -TiAl alloys, which are sensitive to incidental damage, including FOD. The HCF failure stress range is greatly affected by FOD, even by very small cracks [12,13], as is also shown by the present results, see figure 8b.

In view of having to account for small cracks, an obvious alternative HCF design approach is to try and use K-T diagrams [15]. Figure 9 shows a generic K-T diagram, including a modification by El Haddad *et al.* [22]. The intention of a K-T diagram is to define and distinguish between regions of *crack growth* and *no crack growth* in HCF. In the first instance, the boundaries between these regions are supposed to be given by the HCF endurance limit for smooth, uncracked specimens, ΔS_e , and a slant line representing fatigue failure stress ranges, ΔS , calculated from combinations of the long crack fatigue crack growth threshold, ΔK_{th} , and characteristic crack sizes. However, to capture small crack growth behaviour below ΔK_{th} (already observed by Kitagawa and Takahashi [15]) El Haddad *et al.* proposed an empirical expression for ΔS , whereby an effective crack size is added to the actual crack size [22]. This empirical expression is given by:

$$\Delta S = \frac{\Delta K_{th}}{Y\sqrt{\pi(a+a_0)}} \quad ; \quad a_0 = \left(\frac{\Delta K_{th}}{Y\Delta S_e} \right)^2 \cdot \frac{1}{\pi} \quad (2)$$

where ΔS , ΔS_e and ΔK_{th} are as defined above; Y is a crack geometry factor; a is the actual defining crack size; and a_0 is the effective crack size to be added to the actual crack size.

Figure 10 shows modified K-T diagrams for the HCF and FOD + HCF specimens:

- Figure 10a is a “first attempt” K-T diagram. This uses the long crack ΔK_{th} for the ABB-23 material [23, 24]; the average HCF endurance limit, ΔS_e , for the three HCF specimens listed in table 2; $Y = 0.65$, the shape factor for a semi-circular surface crack in an infinite body [21, 25]; and derivation of the El Haddad *et al.* curve from equations (2).
- Figure 10b shows the FOD + HCF data with El Haddad *et al.* curves obtained with different values of ΔK_{th} but the same values of ΔS_e and Y . The ΔK_{th} values represent
 - (1) the long crack growth threshold as in figure 10a;
 - (2) the short crack growth threshold, $\Delta K_{th} = 5 \text{ MPa}\sqrt{\text{m}}$, when the crack is microstructurally long, i.e. larger than the lamellar colony size;

- (3) the microstructurally short crack growth threshold, $\Delta K_{th} = 3.2 \text{ MPa}\sqrt{\text{m}}$, when the crack is smaller than the lamellar colony size ($350 \pm 100 \mu\text{m}$).

The values of both short crack growth thresholds were estimated from Kruzic *et al.* [26].

It is seen from figure 10b that the FOD + HCF failure data are only just captured by the empirical curve derived from the microstructurally short fatigue crack growth threshold. Taking the results in figure 10 as a whole, it is clear that modified K-T diagrams have difficulty in capturing the FOD + HCF data, even though the data have an orderly trend. There are several possible reasons for this difficulty:

- Subsurface FOD cracks unoxidised by heat-tinting but capable of linking up quickly with the main crack.
- Microstructural damage ahead of the main crack.
- Residual tensile stresses near the FOD indent.
- The stress concentration from the indent.

The stress concentration effect of the indents is quantifiable for cracks emanating directly from the indents [16–18]. It turns out that the data points for the three smallest cracks in figure 10 have been lowered by 20 – 50 MPa owing to the indents. Nevertheless, this does not alleviate the difficulty in capturing FOD + HCF data, since all detrimental influences on the fatigue failure stress ranges of the test specimens would likely be present for in-service FOD.

5. Concluding remarks and recommendations

A proof-of-concept investigation was done to determine whether Kitagawa-Takahashi (K-T) diagrams could provide an alternative HCF design approach for γ -TiAl alloys subjected to Foreign Object Damage (FOD). In the first instance the results were encouraging because the HCF fatigue failure stresses correlated well with the Murakami [20,21] equivalent crack sizes of FOD-induced irregular cracks.

However, even a conservatively modified K-T diagram had difficulty in capturing data representing FOD + HCF failure stress ranges *versus* equivalent crack sizes. This means it will be difficult to provide secure but not excessively conservative boundaries between HCF *crack growth* and *no crack growth* for FOD-damaged γ -TiAl alloys.

In the light of these contrary results, and because the number of definitive tests was unavoidably limited, it is recommended to do a more extensive investigation. More FOD + HCF tests should be done, especially considering an alloy with higher boron content and less coarse microstructure, and also elevated temperature HCF. Further, it is recommended to do fatigue crack growth tests on the same material to measure both short and long fatigue crack growth rates and estimate fatigue crack growth thresholds.

6. Acknowledgements

This investigation was partly sponsored by the Netherlands Agency for Aerospace Programmes (NIVR). Supply of the γ -TiAl material by ALSTOM Power (Switzerland) is much appreciated.

7. References

- [1] Kim, Y.W., Dimiduk, D.M., 191, Progress in the understanding of gamma titanium aluminides, *Journal of Metals*, Vol. 43, pp. 40-47.
- [2] Kim, Y.W., Dimiduk, D.M., 1993, Deformation and fracture behaviour of gamma titanium aluminides, In: 7th International Symposium, Aspects of High Temperature Deformation and Fracture in Crystalline Materials (editor Y. Hosoi), Japan Institute of Metals, pp. 373-382.
- [3] Kim, Y.W., 1994, Ordered intermetallic alloys, part III: gamma titanium aluminides, *Journal of Metals*, Vol. 46, pp.30-39.
- [4] Dolley, Jr., E.J., Ashbaugh, N.E., Worth, B.D., 1996, Isothermal high-cycle-fatigue of a Ti-46.5Al-3.0Nb-2.1Cr-0.2W (at.%) gamma titanium aluminide, In: *Fatigue '96* (editors G. Lütjering and H. Nowack), Pergamon Press, Vol. III, pp.1755-1760.
- [5] Cheng, T.T., Willis, M.R., Jones, I.P., 1999, Effects of major alloying additions on the microstructure and mechanical properties of γ -TiAl, *Intermetallics*, Vol. 7, pp. 89-99.
- [6] Recina, V., 2000, Mechanical properties of gamma titanium aluminides, Thesis, Department of Engineering Metals, Chalmers University of Technology, Göteborg, Sweden.
- [7] Austin, C.M., Kelly, T.J., 1996, Gas turbine engine implementation of gamma titanium aluminide, In: *Superalloys 1996* (editors R.D. Kissinger, D.J. Deye, D.L. Anton, A.D. Cetel, M.V. Nathal, T.M. Pollock and D.A. Woodford), The Minerals, Metals and Materials Society, pp. 539-543.
- [8] Davidson, D.E., 1996, Designing with gamma titanium, CAESAR program: titanium aluminide component applications, In: *Superalloys 1996* (editors R.D. Kissinger, D.J. Deye, D.L. Anton, A.D. Cetel, M.V. Nathal, T.M. Pollock and D.A. Woodford), The Minerals, Metals and Materials Society, pp. 545-553.
- [9] Loria, E.A., 2001, Quo vadis gamma titanium aluminide, *Intermetallics*, Vol. 9, pp. 997- 1001.
- [10] Ritchie, R.O., 1999, The importance of small fatigue cracks in advanced materials, In: *Small Fatigue Cracks: Mechanics, Mechanisms and Applications* (editors K.S. Ravichandran, R.O. Ritchie and Y. Murakami), Elsevier Science, pp.233-245.
- [11] Cowles, B.A., 1996, High cycle fatigue in aircraft gas turbines – an industry perspective, *International Journal of Fracture*, Vol. 80, pp. 147-163.
- [12] Harding, T.S., Jones, J.W., 2000, Fatigue thresholds of cracks resulting from impact damage to γ -TiAl, *Scripta Materialia*, Vol. 43, pp. 623-629.
- [13] Smith, R., Harding, T., Jones, J.W., Steif, P., Pollock, T.M., 2001, The role of impact damage and fatigue strength reduction in gamma titanium aluminide alloys, In: *Structural Intermetallics 2001* (editors K.J. Hemker, D.M. Dimiduk, H.Clemens, R. Darolia, H. Inui, J.M. Larsen, V.K. Sikka, M. Thomas and J.D. Whittenberger), The Minerals, Metals and Materials Society, pp. 259-268.

- [14] Draper, S.L., Lerch, B.A., Pereira, J.M., Nathal, M.V., Nazmy, M.Y., Staubli, M., Clemens, D.R., 2001, Effect of impact damage on the fatigue response of TiAl alloy– ABB-2, In: Structural Intermetallics 2001 (editors K.J. Hemker, D.M. Dimiduk, H. Clemens, R. Darolia, H. Inui, J.M. Larsen, V.K. Sikka, M. Thomas and J.D. Whittenberger), The Minerals, Metals and Materials Society, pp. 295-304.
- [15] Kitagawa, H., Takahashi, S., 1976, Applicability of fracture mechanics to very small cracks or the cracks in the early stage, In: Proceedings of the Second International Conference on Mechanical Behaviour of Materials, American Society for Metals, pp. 627-631.
- [16] Peters, J.O., Ritchie, R.O., 2000, Influence of foreign-object damage on crack initiation and early crack growth during high-cycle fatigue of Ti-6Al-4V, Engineering Fracture Mechanics, Vol. 67, pp. 193-207.
- [17] Peters, J.O., Roder, O., Boyce, B.L., Thompson, A.W., Ritchie, R.O., 2000, Role of foreign-object damage on thresholds for high-cycle fatigue in Ti-6Al-4V, Metallurgical and Materials Transactions A, Vol. 31A, pp. 1571-1583.
- [18] Peters, J.O., Ritchie, R.O., 2001, Foreign-object damage and high-cycle fatigue of Ti- 6Al-4V, Materials Science and Engineering A, Vol. A319-321, pp.597-601.
- [19] Bellows, R.S., Muju, S., Nicholas, T., 1999, Validation of the step test method for generating Haigh diagrams for Ti-6Al-4V, International Journal of Fatigue, Vol. 21, pp. 687-697.
- [20] Murakami, Y., 1987, In: Stress Intensity Factors Handbook (editors Y. Murakami, S. Aoki, N. Hasebe, Y. Itoh, H. Miyata, N. Miyazaki, H. Terada, K. Tohgo, M. Toya and R. Yuuki), Pergamon Press, Vol. 2, pp. 822-832.
- [21] Murakami, Y., 1985, Analysis of stress intensity factors of modes I, II and III for inclined surface cracks of arbitrary shape, Engineering Fracture Mechanics, Vol. 22, pp. 101-114.
- [22] El Haddad, M.H., Smith, K.N., Topper, T.H., 1979, Fatigue crack propagation of short cracks, Journal of Engineering Materials and Technology, Vol. 101, pp. 42-45.
- [23] Nazmy, M., Lupinc, V., 2002, Gamma TiAl intermetallic for turbomachinery applications, In: Materials for Advanced Power Engineering 2002 (editors J. Lecomte- Beckers, M. Carton, F. Schubert and P.J. Ennis), Forschungszentrum Jülich GmbH, Part I, pp. 43-56.
- [24] Lupinc, V., Marchionni, M., Nazmy, M., Onofrio, G., Staubli, M., Tomasi, A., 2002, Mechanical properties and oxidation behaviour of a cast TiAl intermetallic, In: Materials for Advanced Power Engineering 2002 (editors J. Lecomte-Beckers, M. Carton, F. Schubert and P.J. Ennis), Forschungszentrum Jülich GmbH, Part II, pp. 683-692.
- [25] Lukáš, P., 1987, Stress intensity factor for small notch-emanating cracks, Engineering Fracture Mechanics, Vol. 26, pp. 471-473.
- [26] Kruzic, J.J., Campbell, J.P., Ritchie, R.O., 1999, On the fatigue behaviour of γ -based TiAl: role of small cracks, Acta Materialia, Vol. 47, pp. 801-816.

Table 1 FOD impact test results, using a Scanning Electron Microscope (SEM)

| Specimen | Impact velocity (m/s) | Indent diameter (mm) | Indent depth (mm) | Main damage diameter (mm) |
|----------|-----------------------|----------------------|-------------------|---------------------------|
| 8A | 50 | 1.04 | 0.09 | – |
| 8B | 50 | 1.06 | 0.09 | – |
| 9A | 100 | 1.41 | 0.16 | 1.98 |
| 9B | 100 | 1.43 | 0.17 | 1.93 |
| 4A | 150 | 1.70 | 0.24 | 2.31 |
| 11 | 150 | 1.66 | 0.23 | 2.33 |
| 2 | 200 | 1.86 | 0.30 | 2.51 |
| 3A | 200 | 1.85 | 0.29 | 2.54 |
| 5A | 250 | 2.05 | 0.37 | 3.10 |
| 6A | 250 | * | * | * |

* specimen failed upon impact

Table 2 FOD + HCF test results

| Specimen | Impact velocity (m/s) | ΔS_f (MPa) | ΔS_{f-1} (MPa) | N_f (kilocycles) | ΔS (MPa) |
|----------|-----------------------|--------------------|------------------------|--------------------|------------------|
| 3B | 0 | 383 | 360 | 735 | 377 |
| 5B | 0 | 360 | 342 | 7 | 343 |
| 6B | 0 | 378 | 360 | 0.07 | 360 |
| 8A | 50 | 252 | 234 | 27 | 239 |
| 8B | 50 | 306 | 288 | 16 | 291 |
| 9A | 100 | 252 | 234 | 5 | 235 |
| 9B | 100 | 198 | 180 | 19 | 183 |
| 4A | 150 | 144 | 126 | 16 | 129 |
| 11 | 150 | 144 | 126 | 8 | 127 |
| 2 | 200 | 81 | * | 0.831 | 81 |
| 3A | 200 | 144 | 126 | 53 | 136 |
| 5A | 250 | 32 | * | 1.922 | 32 |

* specimens failed in first block of cycles

Table 3 FOD-induced crack characteristics and equivalent semi-circular crack diameters perpendicular to the HCF loading axis

| Specimen | Impact velocity (m/s) | Number of cracks | Main crack area (mm ²) | Inclination (degrees) | Equivalent diameter (mm) |
|----------|-----------------------|------------------|------------------------------------|-----------------------|--------------------------|
| 8A | 50 | 1 | 0.0088 | 25 | 0.149 |
| 8B | 50 | 0 | – | – | – |
| 9A | 100 | 1 | 0.0214 | 30 | 0.233 |
| 9B | 100 | 2 | 0.1216 | 9 | 0.556 |
| 4A | 150 | 2 | 1.3923 | 14 | 1.883 |
| 11 | 150 | 1 | 1.3104 | 15 | 1.827 |
| 2 | 200 | 1 | 5.2431 | 10 | 3.654 |
| 3A | 200 | 1 | 0.8457 | 10 | 1.467 |
| 5A | 250 | * | * | 18 | * |

* crack covered about 75% of total fracture surface and therefore excluded from analysis

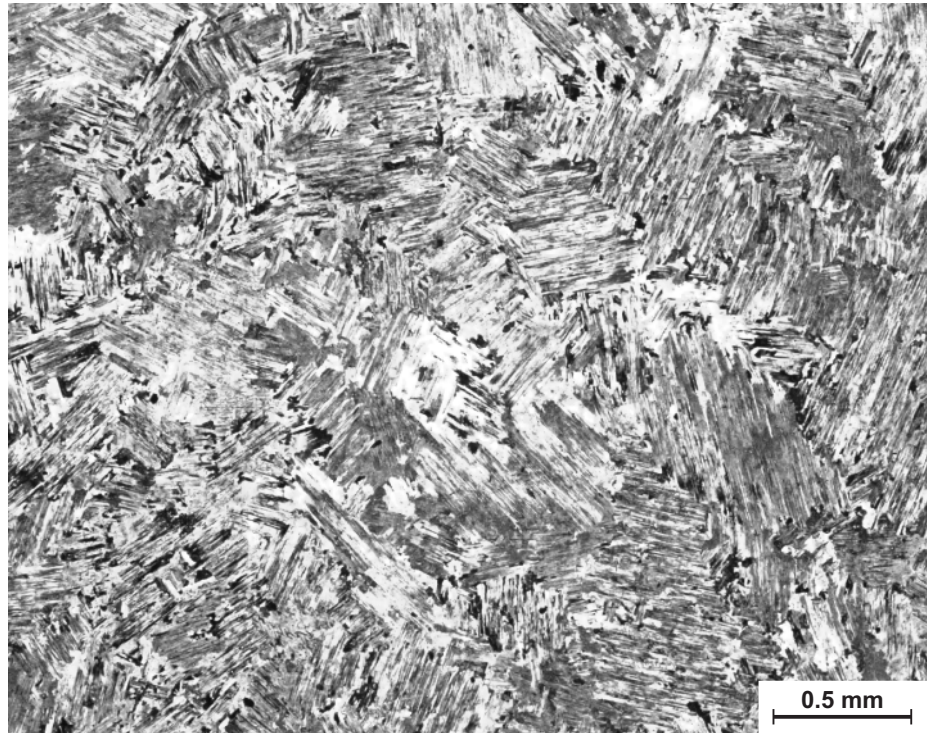


Fig. 1 Representative microstructure of the ABB-23 blade: optical micrograph

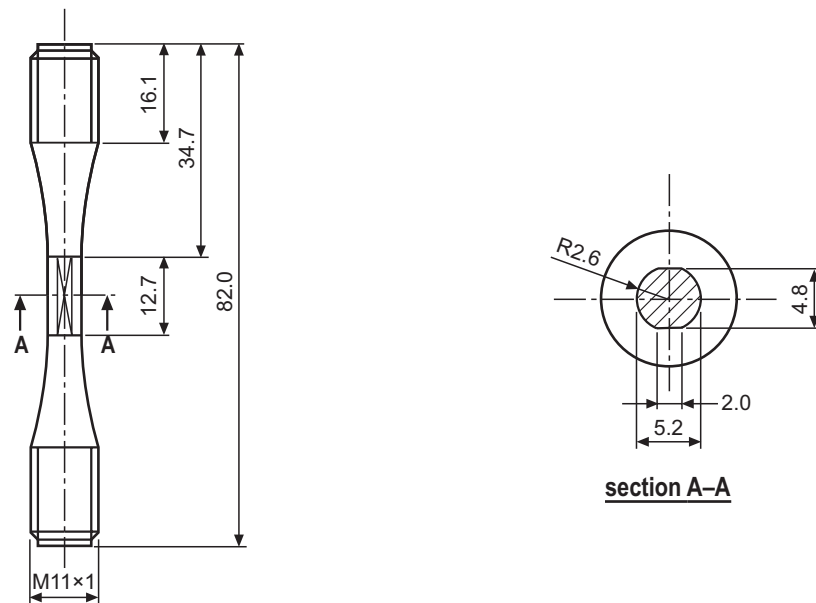


Fig. 2 FOD + HCF specimen design: dimensions in mm



Fig. 3 FOD + HCF specimen in support fixture before impact testing. The back of the specimen is supported by a cork sheet

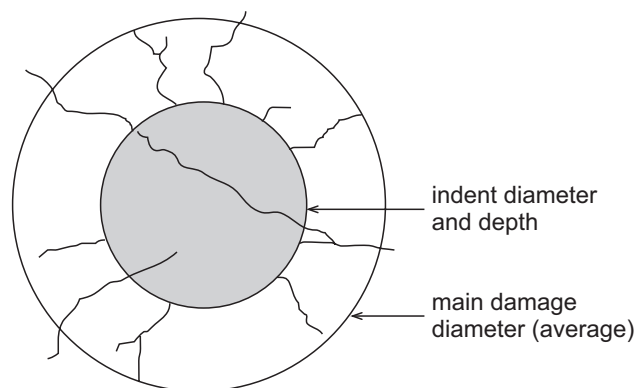


Fig. 4 Schematic of quantifying FOD from the definitive impact tests

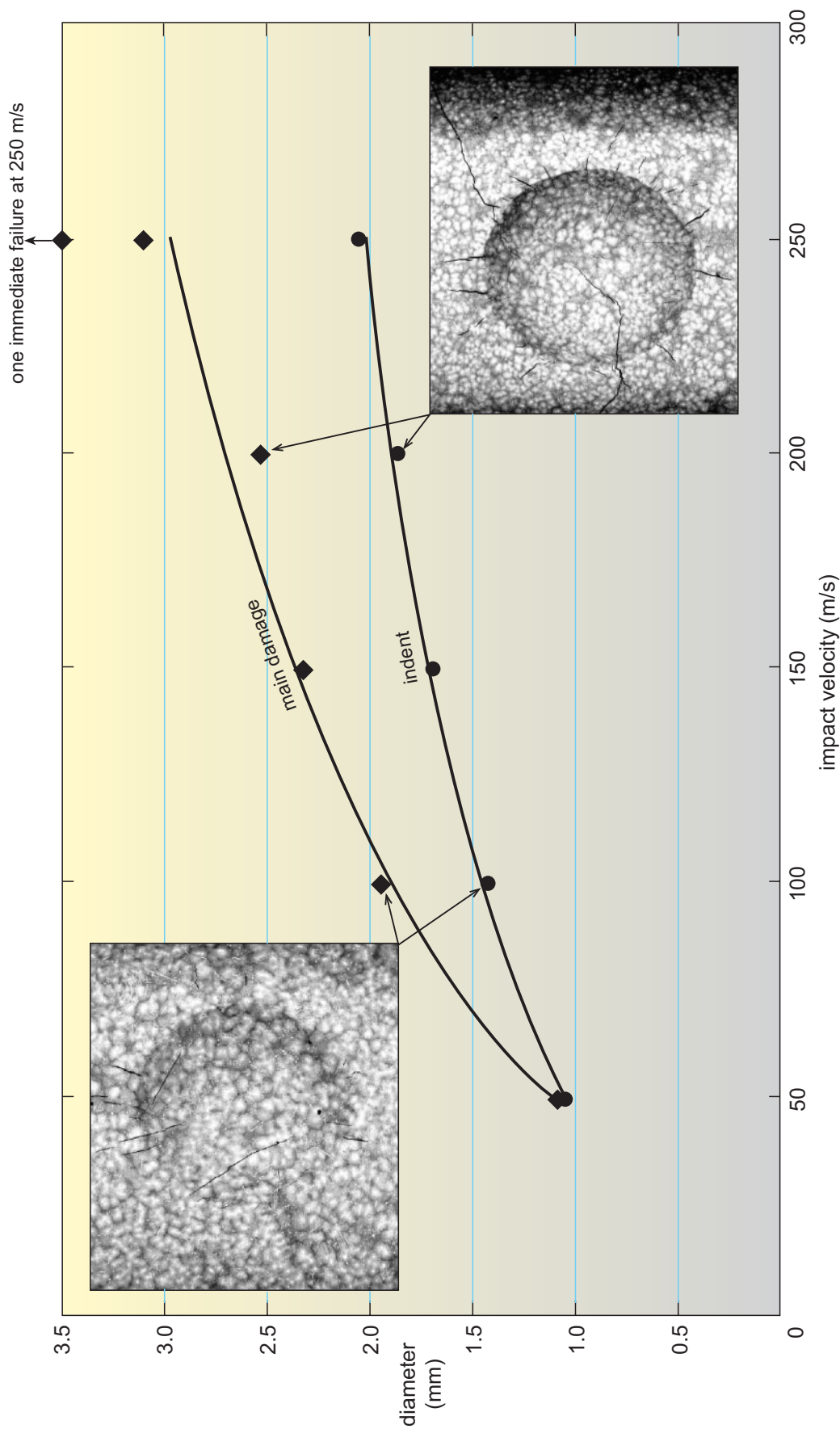


Fig. 5 Dependence of indent and main damage diameters on impact velocity, and two examples (100 m/s and 200 m/s) showing indents and cracks in a γ -TiAl FOD + HCF specimen. Data from table 1

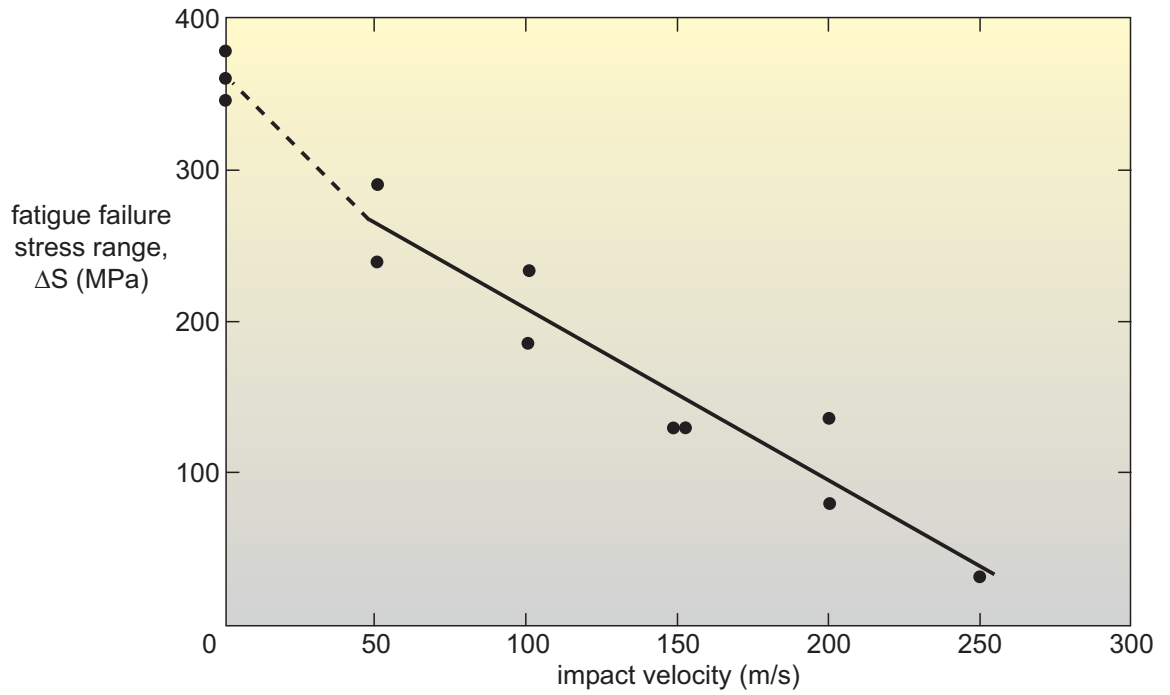


Fig. 6 HCF fatigue failure stresses for HCF and FOD + HCF specimens

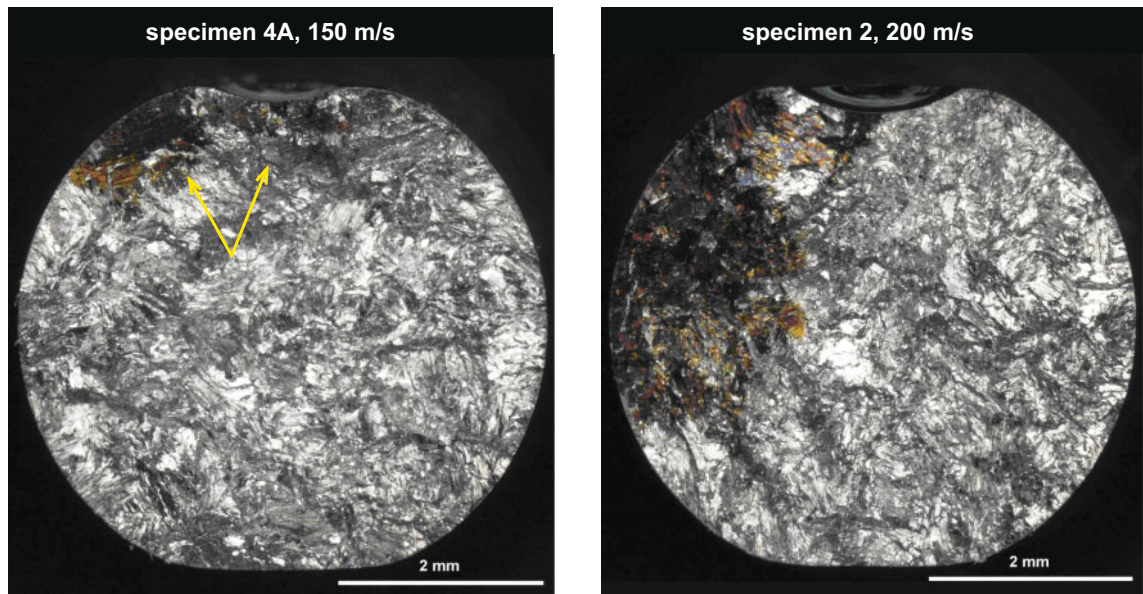


Fig. 7 Examples of FOD-induced heat-tinted cracks after specimen HCF failure

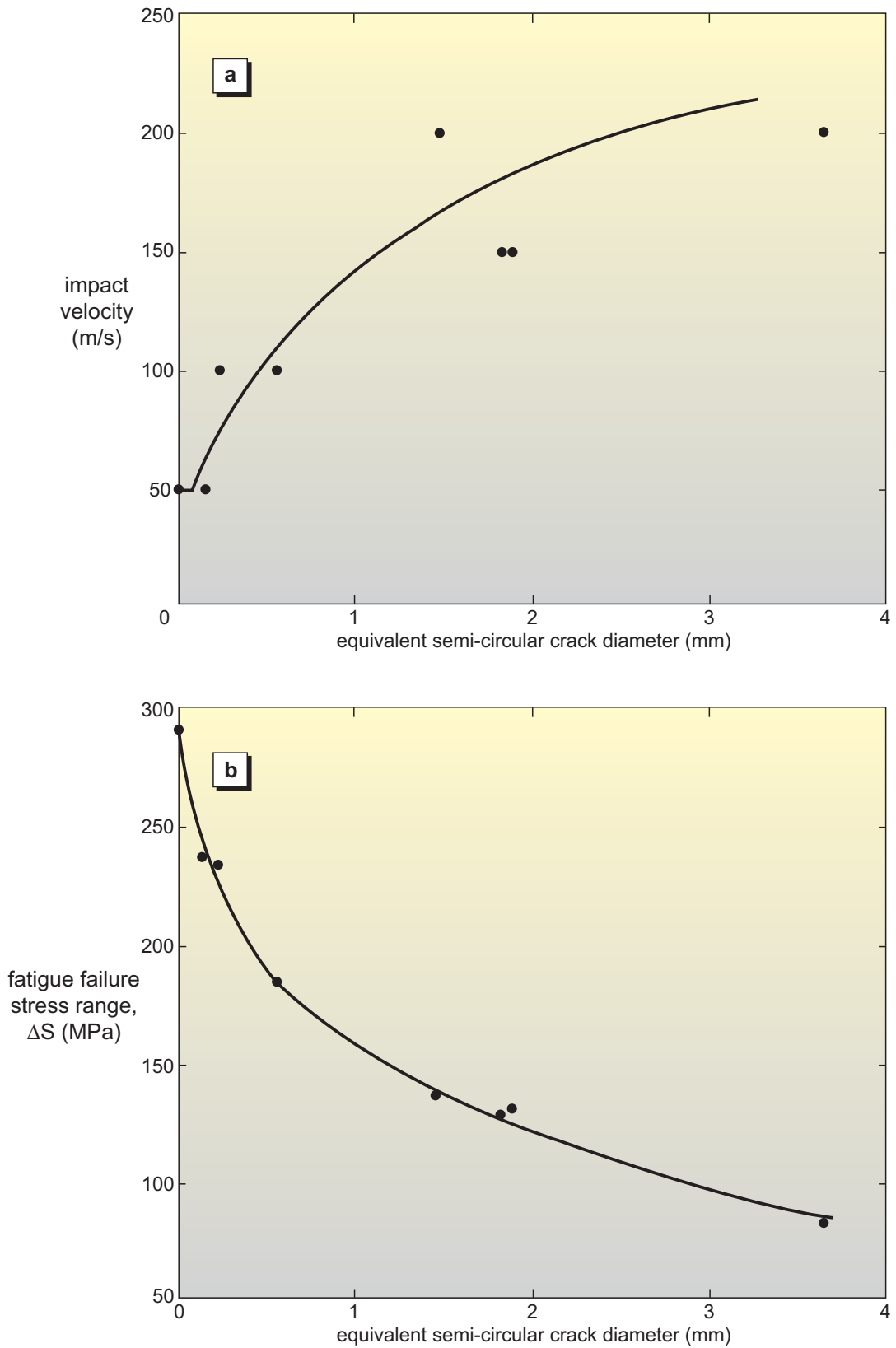


Fig. 8 Impact velocities and HCF fatigue failure stresses versus equivalent FOD-induced crack sizes

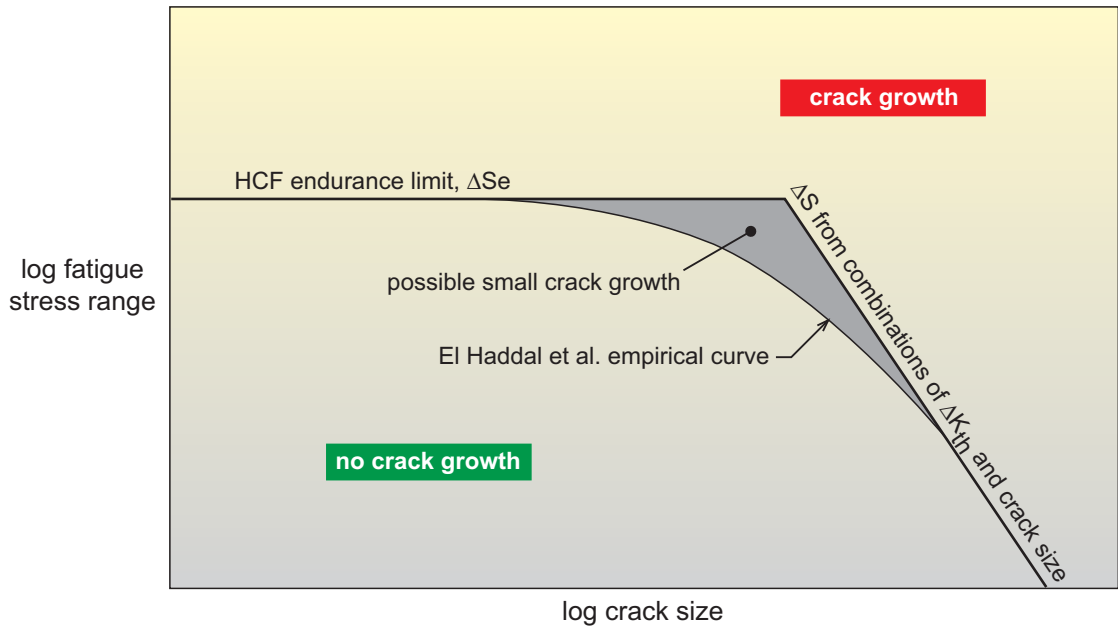


Fig. 9 Generic illustration of a (modified) Kitagawa-Takahashi diagram

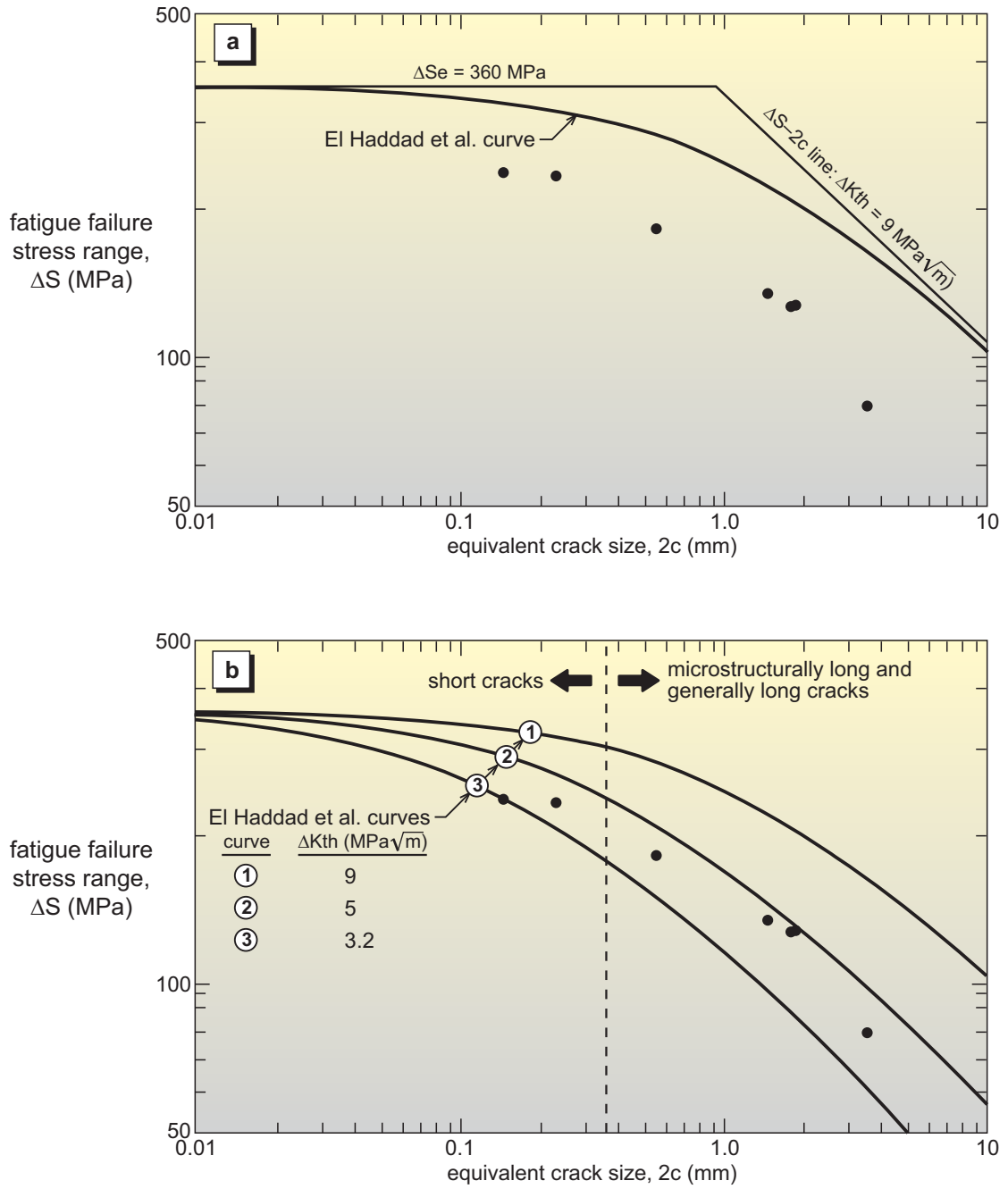


Fig. 10 Modified Kitagawa-Takahashi diagrams for the HCF and FOD + HCF specimens: see text for explanation of the diagrams